In-Situ Exfoliation of Graphene in Epoxy Resins:

a Facile Strategy to Efficient and Large Scale Graphene Nanocomposites

Yan Li [1], Han Zhang [1,2], Maria Crespo [1], Harshit Porwal [1,2], Olivier Picot [1,2], Giovanni Santagiuliana [1], Zhaohui Huang [3], Ettore Barbieri [1,2], Nicola M. Pugno [4,5,1], Ton Peijs [1,2], Emiliano Bilotti [1,2*]*

[1] School of Engineering and Materials Science, Queen Mary University of London, Mile End Road, E1 4NS, London, UK

[2] Nanoforce Technology Ltd., Mile End Road, E1 4NS London, UK

[3] School of Materials Science and Technology, China University of Geosciences, 100083, P. R. China

[4] Laboratory of Bio-inspired & Graphene Nanomechanics, Department of Civil, Environmental and Mechanical Engineering, University of Trento, Via Mesiano 77, 38123 Trento, Italy

[5] Center for Materials and Microsystems, Fondazione Bruno Kessler, Via Sommarive 18, 38123 Povo, TN, Italy

*Email: e.bilotti@qmul.ac.uk, t.peijs@qmul.ac.uk

KEYWORDS: *In-situ* Exfoliation, Graphene, Epoxy Resins, Three Roll Mill, Nanocomposites

ABSTRACT

Any industrial application aiming at exploiting the exceptional properties of graphene in composites or coatings is currently limited by finding viable production methods for large volumes of good quality and high aspect ratio graphene, few layer graphene (FLG) or graphite nanoplatelets (GNP). Final properties of the resulting composites are inherently related to those of the initial graphitic nanoparticles, which typically depend on time-consuming, resource-demanding and/or low yield liquid exfoliation processes. In addition, efficient dispersion of these nanofillers in polymer matrices, and their interaction, is of paramount importance. Here we show that it is possible to produce graphene/epoxy nanocomposites *in-situ* and with high conversion of graphite to FLG/GNP through the process of three-roll milling (TRM), without the need of any additives, solvents, compatibilisers or chemical treatments. This readily scalable

production method allows for more than 5 wt.% of natural graphite (NG) to be directly exfoliated into FLG/GNP and dispersed in an epoxy resin. The *in-situ* exfoliated graphitic nanoplatelets, with average aspect ratios of 300-1000 and thicknesses of 5-17 nm, were demonstrated to conferee exceptional enhancements in mechanical and electrical properties to the epoxy resin. The above conclusions are discussed and interpreted in terms of simple analytical models.

INTRODUCTION

As vastly reported, graphene´s superb properties (theoretical specific area of *ca*. 2360 m^2/g,[1] thermal conductivity of ~5000 $W \cdot m^{-1} \cdot k^{-1}$,[2] intrinsic charge mobility of 200,000 $cm^2 \cdot V^{-1} \cdot s^{-1}$,[3] Young's modulus of ~1.0 TPa and strength of ~130 GPa[4]), impermeability to gas or liquids[5] promise to have significant impact on a host of different industries and advanced application fields such as sensors, optoelectronics, batteries, transparent conductive electrodes/films or energy management.[6-13] However, its industrial adoption will only be possible when a method to produce 'good quality' (i.e. high aspect ratio, minimum thickness, few defects) graphene, few layer graphene (FLG) or graphite nanoplatelets (GNP) at low cost and in large-scale, will be developed.

If graphene is a single layer of sp^2 hybridised C atoms, FLG usually indicates a nanoparticle characterised by a number of graphene layers between 3 and 10 (< 5 nm thickness), which increases to 10 to 100 layers for GNP. Unfortunately the same physical properties (e.g. mechanical, electrical) that make graphene such an exciting material, deteriorate rather swiftly with number of stacked layers. It has been reported for instance that the Young's modulus decreases from 1 TPa to ~ 600 GPa and 400 GPa when going from an isolated graphene particle to a stack of 5 or 10 layers, respectively.[14] The problem is that single layer graphene is very difficult to produce - particularly in the case of large lateral dimensions - as well as to process. In fact it suffers from shape instability as it tends to roll, scroll, wrinkle or fold-up unless it is constrained onto a solid surface.[15] So a difficult compromise between properties, costs and processability has to be faced. FLG/GNP could well represent a more viable alternative to graphene if they could be produced cheaply and with large high aspect ratio as well as being processed easily.

Currently the most promising large scale production method for graphene/FLG/GNP is liquid exfoliation of graphite. Within liquid exfoliation, two possible routes can be distinguished: either graphite is first functionalised (mainly oxidised to produce graphene oxide) before being exfoliated in water[16] or it is directly exfoliated in organic solvents (notably NMP),[17] ionic liquids,[18-19] mixed solvents (acetone/water)[20] or in water/surfactants mixtures,[21-22] via contact or non-contact techniques.[22-23] The oxidising route is very efficient at producing predominantly monolayers and relatively large nanoparticles (50 nm to 3 μm),[24-25] but it introduces large quantities of defects which significantly and irreversibly compromise the physical properties of graphene. Graphene oxide, for instance, has a Young's modulus of about 250 GPa,[26] thermal conductivity of about 18 $W \cdot m^{-1} \cdot k^{-1}$ (46% carbon content),[27] and a low electrical conductivity which, for fully reduced monolayers, can only be partially recovered up to 2 $S \cdot cm^{-1}$, with a field effect mobility of 2−200 $cm^2 \cdot V^{-1} \cdot s^{-1}$ at room temperature.[28] The direct liquid exfoliation of graphite gives rise to nanoplatelets with few defects but with larger thickness (typically between 1 and 10 layers) and limited lateral size (typically between 100 nm to 1 μm). But high boiling point (organic) solvents are costly and difficult to handle and to extract while surfactants can essentially act as contaminants (for instance by limiting the electrical properties) if not carefully extracted. Moreover all liquid exfoliation methods suffer from a number of additional common problems including: low yield (typically 1-3%), use of energy intensive exfoliations techniques (usually ultrasonication but also high shear mixing) and/or long processing time (from several hours to several hundreds of hours) and low concentration of stable graphene/FLG/GNP liquid suspensions (typically up to few mg/ml).[29] Last but not least remains the problem of how to process a relatively low concentrated, only partially stable, graphene/FLG/GNP liquid suspension and convert it into a polymer nanocomposite or other assembly or device. All the above have effectively hindered any real industrial applications.

In order to overcome the above limitations, herein we present for the first time an effective and powerful route to produce *in-situ* exfoliated FLG/GNP directly into the polymer matrix of choice, by three-roll milling (TRM), avoiding any intermediate steps (e.g. filtering, removal of the dispersing liquid medium, purification, drying of powder, redispersion into the final matrix, etc.).

TRM has already been proven very effective in dispersing 1D nanofillers such as carbon nanotubes (CNTs)[30] or 2D nanoparticles such as nanoclays,[31] within epoxy resins. Unfortunately, only limited reports on the dispersion of graphitic materials are present in the scientific literature.[23, 32] Recently Throckmorton *et al.* claimed that TRM is capable to partially exfoliate and disperse graphite into FLG/GNP directly into an epoxy resin but only in presence of an ionic liquid as solvent/dispersant.[33] In absence of the ionic liquid, no electrical conductivity could be even detected for epoxy composites with filler content as high as 3 wt.%.

For the first time we are able to demonstrate that graphite can be efficiently exfoliated and dispersed into an epoxy resin to *in-situ* produce FLG/GNP, without the need of any additives, solvents or compatibilisers and chemical or physical pre-treatments. This work presents a complete study of the relationship between TRM conditions, the structure/property of high-quality FLG/GNP and the properties achieved on the final nanocomposites, interpreted in terms of simple energy balances and geometrical arguments, a numerical model of the TRM process and the Hansen solubility parameters. Careful control over the TRM parameters results in relatively large aspect ratio FLG/GNP (up to 1000) combined with a relatively minimal thickness (minimum average thickness 5 nm) and, notably, 100 % conversion from the starting natural graphite powder.

EXPERIMENTAL

Materials

Natural graphite flakes (NG) were purchased from Alfa Aesar (Product No. 43319). The MVR444 two-part epoxy resin was supplied by Cytec (UK).

Exfoliation and dispersion protocols

Dispersions with various NG contents were prepared using a three-roll mill (80E EXAKT GmbH, Germany). The process was done in three steps: **i)** the NG powder was pre-dispersed in the epoxy resin at 70 ^{o}C for 10 min using a magnetic stirrer to produce: **a)** composites with concentrations of 1, 2, 3, 4 and 5 wt.% and **b)** a 5 wt.% masterbatch; **ii)** this masterbatch was then diluted to the desired final loading (1 to 4 wt.%) for sake of comparison and **iii)** finally, all prepared samples were fed into the TRM. In a typical experiment, the epoxy/NG mixture was

passed 8-10 consecutive times through the TRM (referred to as 8-10 cycles), whereby the speed and roll-to-roll distance (gap size) as well as temperature were varied. A summary of the five different processing parameters is given in the Supporting Information (**Table S3 and S4**).

The final particle sizes were found to be affected predominantly by only two parameters: a) shear loading (controlled mainly by roll speed and gap size) and b) temperature. For sake of simplicity we will focus only on these two parameters which will be discussed separately in section 3.1, by analysing three series of samples following: Protocol I, II and III.

- Protocol I includes up to ten cycles, all done at a fixed gap distance of and fixed NG concentration (5 wt.%). The rotation speed of the apron roll was progressively increased from 30 to 60, 90, 150 and 200 rpm every two cycles.

- Protocol II includes up to eight cycles, with the same rotational speed (200 rpm) of the apron roll for all cycles and fixed NG concentration (5 wt.%). During Protocol II, the epoxy/NG mixtures were passed through the TRM twice in gap mode (fixed roll-to-roll distance) and then six cycles in force mode (fixed applied force of 5.0 N/mm) both done by using a ratio of 1:3:9 between N_1 (feed roller) : N_2 (central roller) : N_3 (apron roller). During the first cycle in gap mode, gaps of N_1/N_2 = 120 µm and N_2/N_3 = 40 µm were used. For the second cycle, N_1/N_2 and N_2/N_3 were reduced to 60 and 20 µm, respectively.

- Protocol III utilized the same process parameters of Protocol II except for the resin temperature, which was varied between 25 °C and 40 °C. 4 and 5 wt% graphite were added to epoxy for exfoliation via Protocol III.

Fabrication of epoxy nanocomposites

After the exfoliation/dispersion conditions following Protocol I, II and III, the hardener was added to the epoxy in a 58:100 ratio after exfoliation/dispersion. The mixtures were degassed under gentle mechanical stirring at 70 ^{o}C for 60 min in a vacuum chamber (pressure of -1 bar). Mixtures were then casted into stainless steel moulds at room temperature and cured in an oven. The following curing conditions were applied: **i)** temperature ramp from RT to 120 ^{o}C (3 ^{o}C·min^{-1}) followed by a 90 min isotherm, **ii)** temperature ramp from 120 ^{o}C to 180 ^{o}C at

(3 $^{o}C \cdot min^{-1}$) followed by a 180 min isotherm and **iii)** cooling down from 180 ^{o}C to RT at 3 $^{o}C \cdot min^{-1}$.

Characterisation techniques

Morphological studies were carried out using optical microscopy (OM, Olympus BX 60) and/or scanning electron microscopy (FEI, Inspector-F) with an electron beam of 20 kV. SEM was conducted to assess the morphology and in particular the length (defined as the longest lateral dimension) of the particles. Specimens were prepared by "extracting" the particles from the different dispersions straight after TRM. Typically, a small amount of uncured epoxy/particle dispersion was immersed in acetone to dissolve the epoxy, followed by filtration using a 0.2 μm PA6 membrane. The obtained particles were then washed three times to remove any remaining epoxy, which was confirmed by optical microscopy. These particles were re-dispersed in acetone to a final concentration less than 5 $mg \cdot ml^{-1}$. The obtained suspension was casted onto an ITO coated glass substrates without gold coating at RT. After evaporation of acetone, the specimens were imaged as prepared. SEM was then used to estimate the length of the FLG/GNP by measuring 100-120 particles. Average values are reported.

Transmission electron microscopy (TEM) (JOEL JEM-2010) was used to see the morphology and different degrees of the exfoliated graphene. The FLG/GNP particles, extracted from uncured liquid epoxy according to the method described in the previous above, were dispersed in acetone (typical concentration 0.05 mg/ml) before being deposited on TEM grids (300 mesh, 3 mm, purchased from TAAB, C267/050) by drop casting. The copper grid with graphene dispersion was dried at RT for 10 min. 10-15 representative particles were collected for each specimen. The thickness of the FLG/GNP particles is estimated from the thickness of the edge of the particles sticking out of the plane of the copper grid.

Raman spectroscopy (Nicolet Almega XR, High-Performance Dispersive Raman Spectrometer) was utilized to characterise of natural graphite, exfoliated GNP. GNP sheet was prepared by vacuum filtration of the dispersion through a porous membrane (PVDF, pore size 0.45 μm). Raman measurements were performed with a wavelength of 532 nm.

The viscosity of the pure epoxy and the complex viscosity of the graphite/epoxy mixtures were measured by an AR2000 Rheometer equipped with 40 mm steel parallel plates. The

temperature was ramped both up and down at 3 °C·min^{-1} from 25 to 100 °C and between 1-100 Hz, at a shear strain of 1%.

Drop shape analyzer (DSA100 KRÜSS, GmbH, Germany) was used to measure the contact angle between the liquid epoxy and a glass substrate. The glass substrates were thoroughly cleaned by acetone. Surface energies were calculated from contact angle data of sessile drops of 10 µL. In order to make experiments easier, we choose ethylene glycol as a non-volatile (boiling point: 197.3 °C) reference solvent, with a surface tension of 47.70 N/m at 20 °C. From the measured contact angles, the surface tension of the epoxy was extracted according to the Young-Laplace equation. For more details please refer to Supporting Information **Figure S5** and section: **Surface tension**.

X-ray diffraction (XRD) (Philips PW 3830 automated powder diffraction) was used to characterize the thickness of exfoliated GNPs within the epoxy composites. The samples were cut into rectangular beams (dimensions 3.2 x 10 x 30 mm^3). The X-ray texture scans were obtained between 2θ = 20-90° at a scanning rate of 1°/min. The average out-of-plane crystallite thickness of the GNPs (t) was estimated using the full width at half maximum (FWHM) of the (002) peak by Scherrer´s equation:

$$t = \frac{K\lambda}{\beta \cos\theta} \qquad \text{Equation 6}$$

where β is the line breadth (FWHM) in radians with the instrumental broadening subtracted, λ is the X-ray wavelength, and θ is the diffraction angle of the (002) peak. The coefficient K was taken to be 0.89 according to Raza *et al.*[34-35] XRD result was the average value of three repetitions.

The conductivity of all samples was measured by a two probes method using a picoammeter (Keithley 6485) and a DC voltage source (Agilet 6614C). Samples were cut into beams of 3.2 x 10 x 30 mm^3 and silver paste was applied to the cross-section to ensure good contact between the electrodes and the sample. Voltages in the range 5 to 10 V were used. For specimens with resistances exceeding 10^{10} Ohm, electrical resistivity was no longer measurable and the samples were considered as ‘non-conductive’. Three specimens for each composite were tested in order to obtain average values of conductivity.

Flexural test specimens were prepared according to the ASTM-D 790 standard. The samples were cut into beams of dimensions 3.2 x 12.7 x 70 mm^3. The cut surfaces were polished by hand using different grade abrasive paper (from 1000 to 4000 grit). The support span to depth ratio was 16:1 and a strain rate of 0.01 mm/min was used.

RESULTS AND DISCUSSION

Effect of shear on *in-situ* exfoliation of natural graphite in epoxy resin

SEM images in **Figure 1.a-b** present the typical morphology of the natural graphite flakes used in this study. With lateral dimensions varying between ~ 600 ± 150 μm and ~ 800 ± 200 μm and a thickness of circa 40 μm, the initial natural graphite flakes present an aspect ratio of circa 20 ± 5. **Figure 1.g** shows a typical graphitic Raman spectra with the G and 2D peaks positioned at, respectively, 1585 cm^{-1} and 2718 cm^{-1}. No D peak (defect) was instead observed due to the high degree of crystallinity.

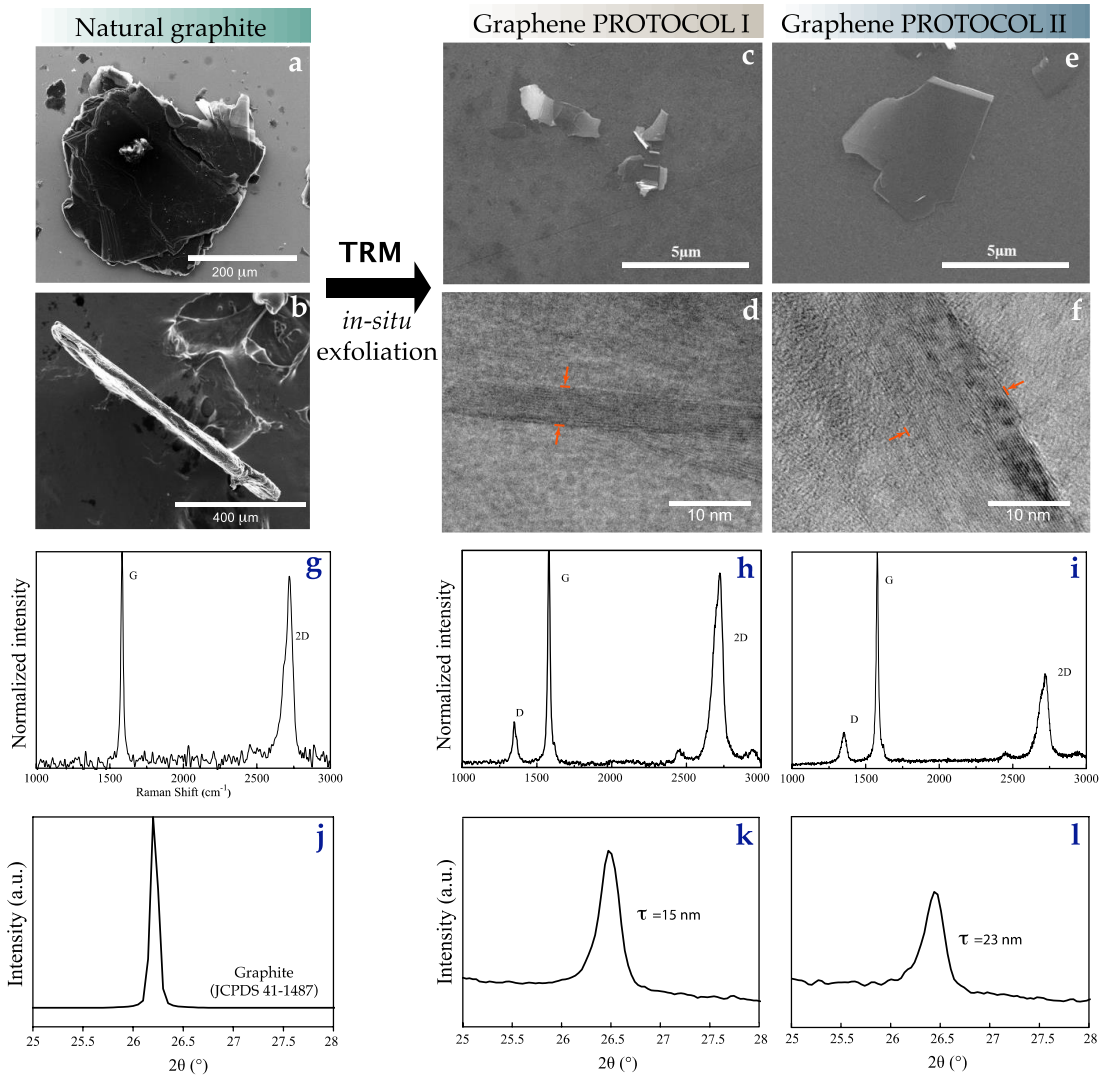

Figure 1. *In-situ* exfoliation of natural graphite (SEM images a and b) by TRM. SEM and TEM images of FLG/GNPs after exfoliation through Protocol I (c and d) and Protocol II (e and f). Comparison of Raman and XRD spectra ($2\theta \approx 26.1°$ indexed to the (0 0 2) planes of a hexagonal graphite lattice) before and after exfoliation: graphite (g and j), FLG/GNP Protocol I (h and k) and FLG/GNP protocol II (i and l), respectively.

After the TRM processes the morphology of the natural graphite changes dramatically. The particle contour changes from relatively smooth and round to mostly sharp edged (**Figure 1.c, Figure 1.e**). Both lateral dimensions and thickness (**Figure 1.d, Figure 1.f**) are reduced but, interestingly, not in the same proportion. The platelet thickness is reduced by

approximately three orders of magnitude, hence demonstrating the success of the *in-situ* exfoliation, while the lateral dimension is reduced by about two orders of magnitude [34].

Table 1 summarises the average particle dimensions calculated from a statistical analysis of the SEM and TEM images and the X-ray data in **Figure 1**. An obvious difference in size of the graphitic particles obtained by the two processing protocols can be observed. Protocol I gives rise to slightly thinner nanoparticles (~ 6 nm instead of ~ 14 nm according to TEM observations). Conversely, Protocol II is able to achieve considerably larger nanoparticles (~ 3.51 μm compared to ~ 0.76 μm). As a result the nanoparticles obtained by Protocol II possess a 3 times higher aspect ratio than those obtained by Protocol I, and 7.5 times higher than of original natural graphite particles. A discrepancy between the values of thickness as measured by TEM and XRD is noticed, consistent with previous reports which explained it in terms of differences in number and quality of sampled particles – which is inherent with the different preparation methods – and as well as the coefficient K selected in the Sherrer equation.[34-35] It is noted that the particles measured by TEM are extracted from uncured liquid resins and drop casted on copper grids from very diluted dispersions. The particles measured by XRD are embedded into the composites after curing the epoxy resins. A partial reagglomeration of particles is expected during curing, which will then result in an increase in the average particle thickness.

For sake of completeness, within this paper we will use both (average) values of thickness, as measured by XRD and TEM, and hence estimate two values of aspect ratio (L/T_{XRD} and L/T_{TEM}) for each protocol.

Figure 1.h-i present also typical Raman spectra for the *in-situ* exfoliated particles obtained by the two protocols. Of interest here is the ratio of the intensities of the D and G bands, I_D/I_G (reported in **Table 1**), which gives indications of the quality of the particles; i.e. the lower the ratio the lower the defects in the graphitic structure. The particles obtained with Protocol II attain a lower I_D/I_G ratio (0.16 instead of 0.20). This difference can be explained by the reduced presence of edge defects for larger flakes (Protocol II), in analogy with previous reports. For instance Khan *et al.* showed a decrease of the I_D/I_G ratio from 0.22 to 0.08 when larger flakes were selectively separated from a solvent dispersion, by decreasing the centrifugation rotational speed from 4000 to 500 rpm.[29]

Table 1. Properties of initial NG and FLG/GNP particles exfoliated according to Protocol I & II.

Sample	Length by SEM L (μm)	Thickness by XRD T_{XRD} (nm)	Thickness by TEM T_{TEM} (nm)	Aspect Ratio (L/ T_{XRD} - L/ T_{TEM})	I_D/I_G (-)
NG	~800	-	~ 40000*	N.A. - ~ 20	0
Protocol I	0.76 ± 0.34	~ 15 ± 3	6 ± 2	50 - 126	0.20 ± 0.05
Protocol II	3.51 ± 0.87	~ 23 ± 2	14 ± 5	150 - 250	0.16 ± 0.08

*estimated from SEM micrographs.

In order to understand the exfoliation process shown above, let us start from a simple energy balance and geometrical argument.

Let us assume initial flakes of sizes L_x, L_y, L_z and define N_x, N_y, N_z as the number of cuts (or delamination, in the case of *z* axis) taking place along the related sides during the exfoliation and thus resulting in a total number of fragments equal to $N = N_x \cdot N_y \cdot N_z$. Indicating with η_f or η_d the energy fractions dissipated, respectively, during (in-plane) fracture of graphene (or other 2D materials) or during (out-of-plane) exfoliation (delamination) to separate the layers, the energy balance imposes $\eta_f + \eta_d = \eta$, where η is the efficiency of the process.

The energy dissipated by fracture is:

$$W_f = \gamma_f L_Z \left(L_x (N_y - 1) + L_y (N_x - 1) \right) \qquad \text{Equation 1}$$

whereas that dissipated by delamination is:

$$W_d = \gamma_d L_x L_y (N_z - 1) \qquad \text{Equation 2}$$

where γ_f or γ_d are the surface energies of fracture or adhesion respectively and *z* is assumed to be perpendicular to the layers. Noting that $N_{x,y,z} >> 1$ and that $L = L_x / N_x$, $W = L_y / N_y$ and $T = L_z / N_z$ are the final lateral sizes *L*, *W* and thickness *T* of the flakes, we find the

following prediction of the flake aspect ratio (λ) during exfoliation (independent from N) imposing the energy balance:

$$\lambda \equiv \frac{\sqrt{LW}}{T} = \frac{\eta_d \gamma_f}{\eta_f \gamma_d} \frac{L/W + 1}{\sqrt{L/W}} \qquad \text{Equation 3}$$

Posing $L/W \approx 1$ (assuming cylindrical nanoplatelets), $\eta_d/\eta_f \approx 1$ (assuming the energy dissipated by fracture is equal to the energy dissipated by exfoliation) and $\gamma_d/\gamma_f \approx 10 - 100$, results in $\lambda \approx 20 - 200$ that is of the order of common experimental observations in the literature. On the other hand, values of λ above 1000 could be achieved if η_d/η_f is above 5-50, in other words if more energy is used for exfoliation (i.e. reduce thickness) rather than fracture (i.e. reduce lateral dimensions). We believe η_d/η_f is intimately linked with the specific processing methods and conditions used. In our case, the fact that Protocol I achieves lower aspect ratio than Protocol II suggests that $(\eta_d/\eta_f)_{Protocol\,I} < (\eta_d/\eta_f)_{Protocol\,II}$. By using the experimental values of aspect ratio found for Protocol I and II (**Table 1**), it is possible to estimate that the ratio η_d / η_f is as high as 2.5 - 6.3 for Protocol I and 7.5 - 12.5 for Protocol II.

But in order to explain the variation in nanoparticle aspect ratio obtained with our different protocols, it is necessary to better understand the actual process. In general it is expected that a higher shear loading should result in more efficient exfoliation, hence thinner graphitic particles. Recently Paton *et al.* [22] demonstrated that well exfoliated FLG/GNP particles could consistently be obtained when shear rates exceeding 10^4 s^{-1} were reached, independently from the mixing method and the dispersing liquid (NMP or water/NaC) used.

In **Figure 2a**, the estimated shear rates achieved in the two TRM Protocols is presented. Shear rates and shear stresses are calculated by modelling the TRM process in analogy to a recent work of Magnier *et al.*,[36] who developed a model to describe the calendering process (in particular the rolls separating force) of power-law non-Newtonian fluids between counter rotating rolls at different velocities. The isothermal model was based on the lubrication approximation, as in classical calendering models.[37] But, due to the asymmetry caused by the different velocities of the rolls, the generalised Reynolds equation had to be solved taking into account various velocities profiles in different zones (4-5 zones). In zone 3, at a certain

horizontal distance $x=x^*$ (please note that x is negative until $x = 0$ at the nip region) before the nip region, in correspondence of a vertical distance (height) between rolls of $2h=2h^*$ (see Supporting Information **Figure. S1**), the pressure is maximum ($dp/dx=0$, see Supporting Information **Figure. S1**) and the velocity profile is linear. Only in this region the shear rate assumes the simple expression:

$$\dot{\gamma} = \frac{U_2 - U_1}{2h^*} \qquad \text{Equation 4}$$

Where U_1 and U_2 are the linear velocities of the two rolls. For a power law non-Newtonian fluid the shear stress can be expressed as:

$$\tau = k(\dot{\gamma})^m \qquad \text{Equation 5}$$

Where m is the power law index and K is the power law coefficient. In our case, K and m have been measured experimentally (see Supporting Information **Figure S3-4**).

Referring back to our process, it is noted that for each cycle the material goes through two gaps (gap 1, between apron roll and central roll, and gap 2, between central roll and feed roll), hence experiencing two different shear rates and shear stresses. Using Equation 4, it can be seen that Protocol I reaches higher shear rates; it effectively always exceeds, at both gaps and for each cycle, the threshold of 10^4 s^{-1} indicated by Paton *et al.* [22], and approaches values of 10^5 s^{-1} in the last 4 cycles. Protocol II, instead, is relatively mild both in terms of shear rates and number of cycles (8 instead of 10). For each cycle, the shear rate at gap 2 never exceeds 10^4 s^{-1} (from 10^3 s^{-1} to 10^4 s^{-1}) while the shear rate at gap 1 progressively increases from 10^4 s^{-1} to $5 \cdot 10^4$ s^{-1}.

Using Equation 5, it can be shown that the shear stress ranges between 5 and 10 MPa, which is well above the minimum resistance of the graphene stack under pure shear (about 0.25 MPa [33]) (**Figure 2b**).

This shows that both protocols should be able to achieve exfoliation of graphite. However, since Protocol I is characterised by higher shear rates, shear stresses and number of cycles,

compared to Protocol II, it is reasonable to expect thinner graphitic nanoparticles, in agreement with experimental observations (**Figure 2, Table 1**).

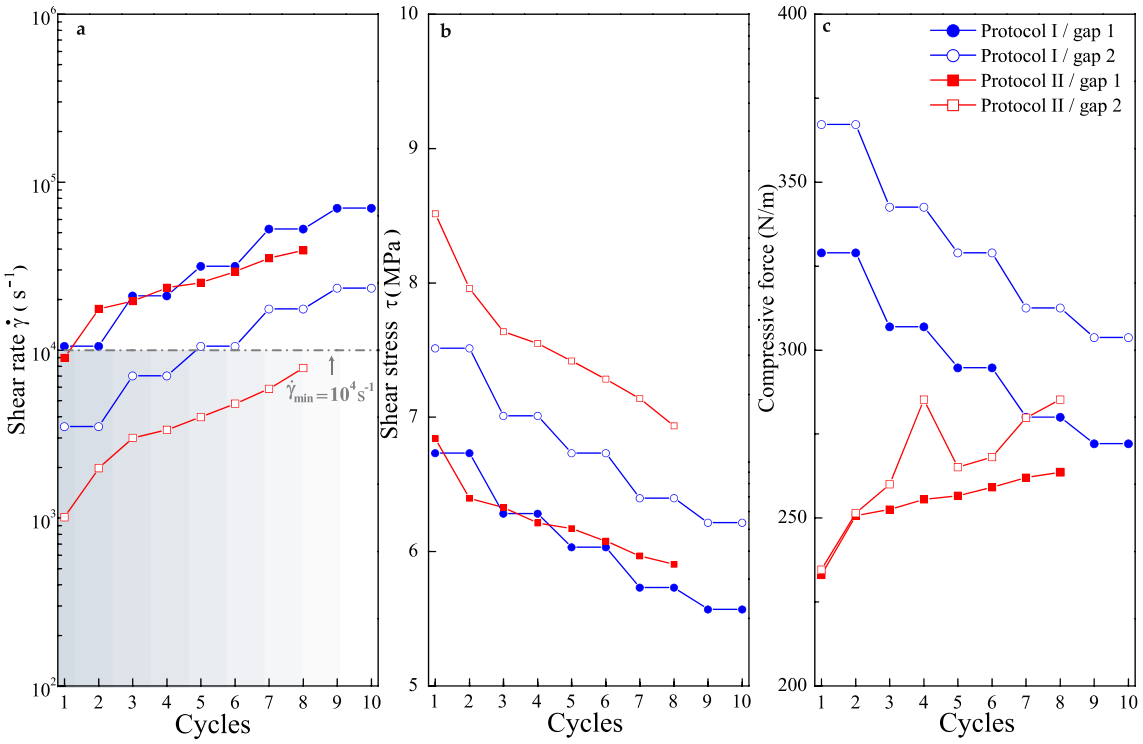

Figure 2. (a) Shear rate (b) Shear stress and (c) compressive force (per unit roll width) experienced by the epoxy composites mixtures as a function of different cycles of Protocol I and II.

Unfortunately more severe processing conditions might also induce breaking down of the graphitic particles (reduction in lateral dimension) along with the reduction of their thickness. In fact it is noted that Protocol I is characterised by much higher compressive forces (**Figure 2c**), particularly at the first cycles, which might induce severe fracturing of the natural graphite particles apart from simple exfoliation. This is in agreement with the previous conclusion $(\eta_d/\eta_f)_{Protocol\ I} < (\eta_d/\eta_f)_{Protocol\ II}$ which states that Protocol I uses a higher fraction of energy for platelet fracture rather than exfoliation, compared with Protocol II.

Effect of temperature on *in-situ* exfoliation of natural graphite in epoxy resin

Another important processing parameter found to significantly affect the *in-situ* exfoliation process was temperature. SEM and TEM micrographs in **Figure 3a-d** show the typical morphology of FLG/GNP particles obtained at different resin temperatures, between 25 °C and 40 °C (Protocol III). The average particle dimensions calculated from a statistical analysis of the SEM and TEM images and the X-ray data are reported in **Table 2**, in analogy with the previous section.

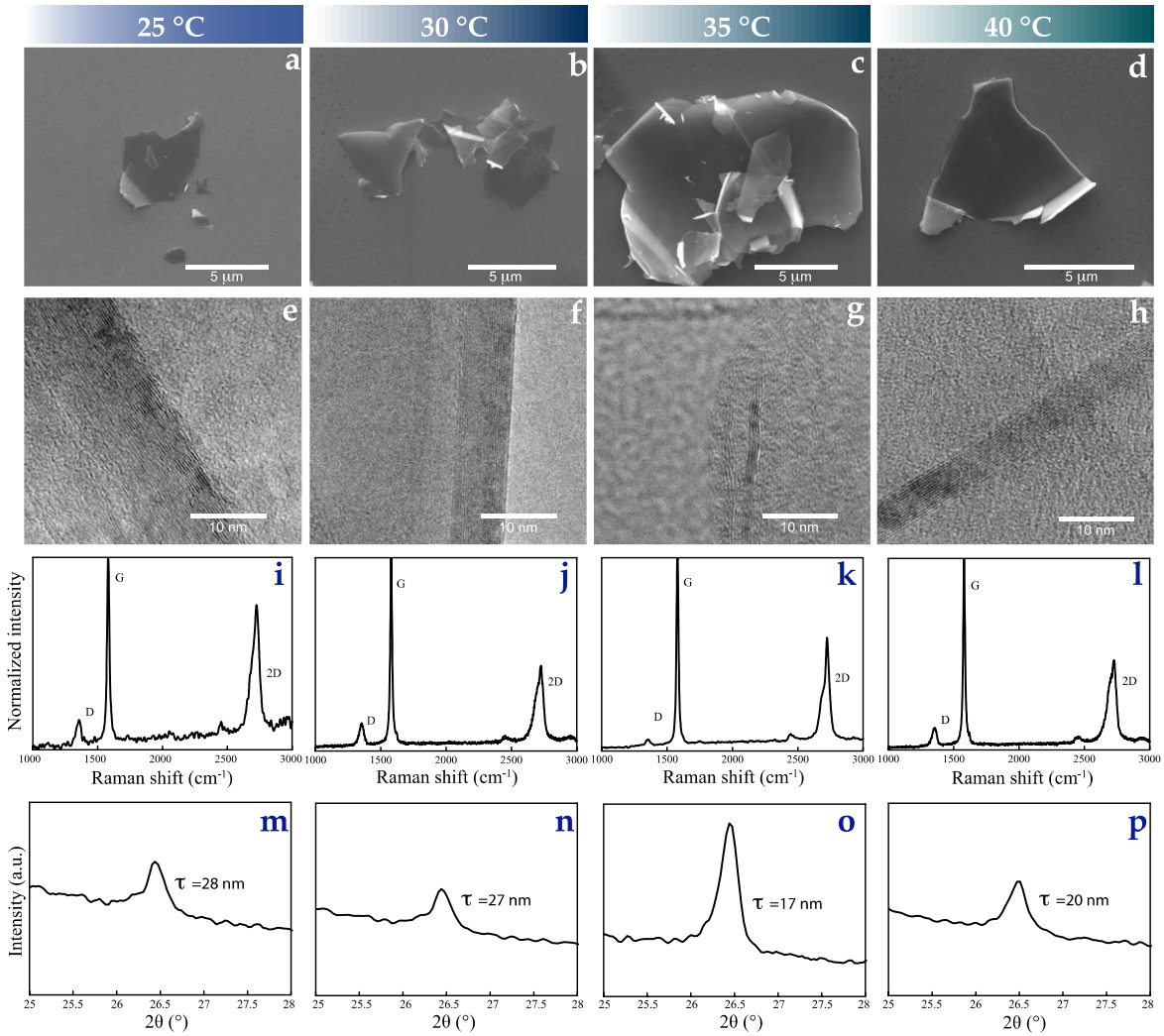

Figure 3. Exfoliation through Protocol III. Effect of resin temperature on morphology (SEM and TEM), Raman spectroscopy and XRD for FLG/GNP produced at: 25 °C (a, e, i and m), 30 °C (b, f, j and n), 35 °C (c, g, k and o) and 40 °C (d, h, l and p), respectively.

Interestingly, the FLG/GNP size strongly depends on processing temperature. Moreover this dependency is non-monotonic. The development of thickness and the lateral dimension experience, respectively, a minimum and a maximum in correspondence of a resin temperature of 35 °C. To the best of the authors' knowledge it is the first time that such an effect is reported. Notably, the FLG/GNP particles obtained at 35 °C reach an aspect ratio of up to 1000, 20 folds larger than Protocol I and 50 folds larger than the original natural graphite particles. **Figure 3.i-l** also presents typical Raman spectra for the *in-situ* exfoliated particles obtained at different temperatures. Also in this case the ratio of the intensities of the D and G bands, I_D/I_G (reported in **Table 2**), is an inverse function of the flakes' lateral dimensions. The I_D/I_G ratio attains a minimum of 0.07 in correspondence of the largest flakes (*in-situ* exfoliated at 35 °C), suggesting a reduction of edge defects.[29]

Table 2. Properties of FLG/GNP particles obtained by Protocol III.

Sample	T (°C)	Length, L (μm)	Thickness by XRD, T_{XRD} (nm)	Thickness by TEM, T_{TEM} (nm)	Aspect Ratio (L/T_{XRD} - L/T_{TEM})	I_D/I_G
Protocol III - 1	25	3.5 ± 1.5	28 ± 8	14 ± 8	125 - 250	0.16 ± 0.08
Protocol III - 2	30	4.0 ± 1.3	27 ± 6	12 ± 4	150 - 333	0.15 ± 0.04
Protocol III - 3	35	5.2 ± 2.0	17 ± 5	5 ± 4	306 - 1040	0.07 ± 0.05
Protocol III - 4	40	4.6 ± 1.8	20 ± 10	9 ± 5	230 - 511	0.12 ± 0.04

In order to explain these exceptional results, it is noted that an increase in temperature monotonically decreases the epoxy viscosity (see Supporting Information **Figure S4**) which, as a consequence, decreases the shear stress for a given shear rate imposed by the TRM process (**Figure 4**). One would therefore expect the exfoliation efficiency to decrease monotonically with increasing temperature, which is in disagreement with the experimental results of **Figure 3** and **Table 2**. Hence, the reduction in viscosity of the epoxy resin cannot explain the difference in *in-situ* exfoliated FLG/GNP particle sizes.

Another physical property which was found to be significantly affected by the temperature was the surface tension of the epoxy resin used. The surface tension, estimated from contact angle measurements (see Supporting Information. **Figure S5** and Section: **Surface**

tension), varied between 65 mJ/m^2 at 25 °C to 30 mJ/m^2 at 40 °C (**Figure 4**). Interestingly, for temperatures between 35-40 °C, the surface tension assumed values of 40 - 50 mJ/m^2, which coincides with the optimal surface tension range for liquids to disperse graphene, as proposed by Hernandez *et al.*.[17] The same authors explained this behaviour by invoking the Hildebrand–Scratchard equation.[38] The latter establishes a relationship between the enthalpy of mixing and the balance of graphene and solvent surface energies, with an energetic minimum expected for solvents whose surface energy matches that of graphene. The same authors could demonstrate and predict the energetic minimum to be in correspondence of a liquid surface tension of 40 - 50 mJ m^{-2}.

In analogy to the work of Hernandez *et al.*[17] we therefore believe that the maximum FLG/GNP aspect ratio found in our case can be explained by a minimisation of the surface energy difference between graphene and the epoxy resin, which assists the *in-situ* exfoliation process. The matching of the surface energy helps dispersing graphene nanoparticles while they are produced by mechanically exfoliation.

Interestingly, the existence of this optimal temperature in Protocol III is in agreement with our previous energetic model introduced in section 3.1, since $\gamma_d \propto \gamma_{\text{graphite}} - \gamma_{\text{resin}} \cos\vartheta$, where ϑ is the contact angle (small under large spreading), is minimized. By using the experimental values of aspect ratio found (**Table 2**), it is possible to estimate that the ratio η_d / η_f is as high as 15 - 50 for Protocol III-3.

Another approach reported in the scientific literature to interpret improved graphene dispersion, apart from the Hildebrand–Scratchard equation, is based on the Hansen solubility parameters (HSP).[20, 39] HSP are widely used to predict the compatibility between two materials.

For each material, three Hansen parameters can be defined: δ_D, δ_P and δ_H, which can be located in the 3D Hansen space just as co-ordinates.[39-40] In the Hansen space a HSP distance R_a, in general between solvent 1 (or any dispersing media) and solute 2 (in our case graphene), can be defined as $R_a = (4(\delta_{D1}-\delta_{D2})^2+(\delta_{P1}-\delta_{P2})^2+(\delta_{H1}-\delta_{H2})^2)^{1/2}$. The smaller R_a, the higher the solubility. In other words a good dispersing media should have HSP matching that of graphene.[41] The HSP of graphene [41] has been estimated as δ_D ~ 18 MPa^{½}, δ_P ~ 9.3 MPa^{½} and δ_H ~ 7.7 MPa^{½}. In a previous publication, using an epoxy resin (bisphenol A-diglycidylether)

similar to the one used in this study, HSP parameters were measured as follows: δ_D ~ 20 MPa^{½}, δ_P ~ 10 MPa^{½} and δ_H ~ 8 MPa^{½}.[42] It is interesting to notice the relative close similarity of the HSP of graphene and epoxy, demonstrating that in general epoxy resins are potentially good dispersing media for graphene. In this paper we build on this relative compatibility and demonstrate that by fine tuning the temperature the dispersability of graphene in epoxy can be further improved, which in turn assists the *in-situ* exfoliation process.

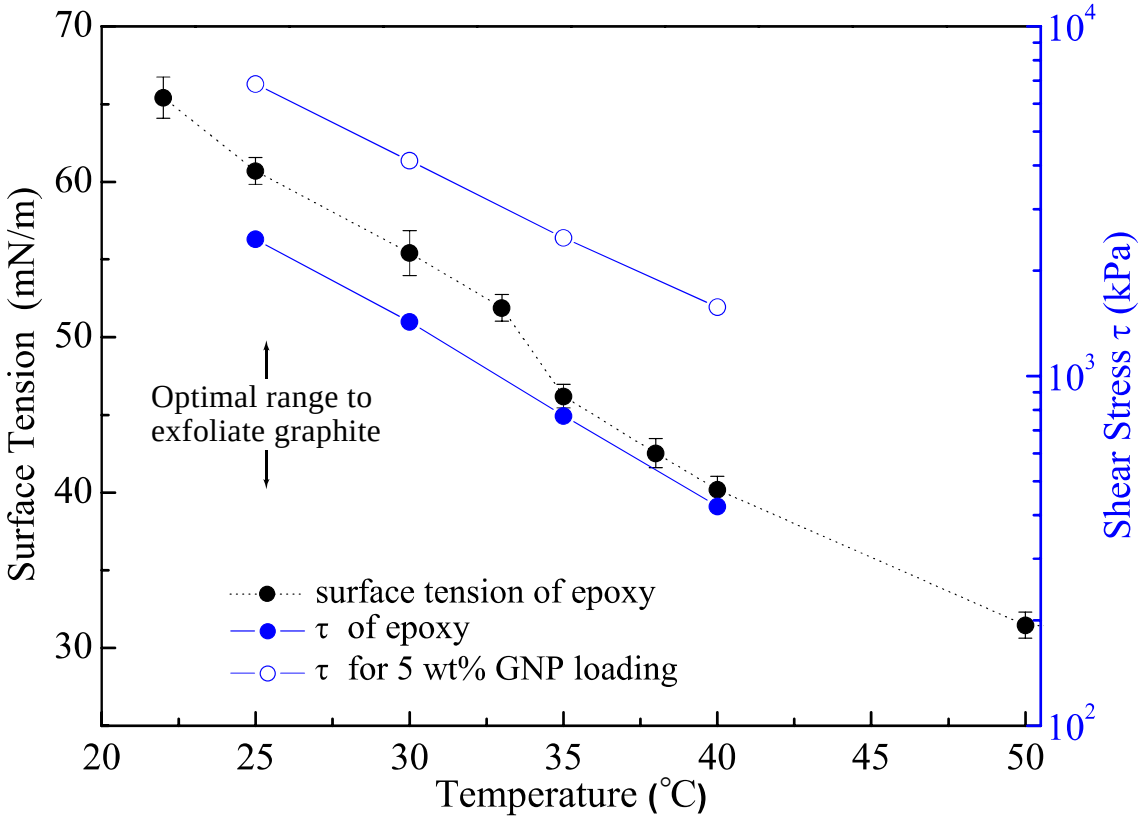

Figure 4. Surface tension and estimated shear stress achieved in Protocol III at different temperatures. The vertical range 40-50 mJ/m^2 represents the optimal range for graphene dispersion/exfoliation in liquids.

Effect of *in-situ* exfoliation on epoxy nanocomposites properties

As explained in the introduction section, in order to fully exploit the potential of graphene or graphitic nanoparticles in a number of application fields including composites and coatings,

it is necessary to produce thin (< 10 layers, preferably < 3-5 layers) and large nanoparticles (aspect ratios > 1000, preferably > 10000)[43] at an industrial-scale. In fact, it is well known from micromechanical composite theories[44] and percolation theories[45-46] that the larger the filler aspect ratio, the higher the mechanical reinforcement is (asymptotically approaching the rule-of-mixture limit), as well as the electrical and thermal conductivity, and the lower the percolation threshold. The filler aspect ratio also plays a fundamental role in a number of other properties, particularly in transport-dominated properties like gas/liquid barrier properties,[47] fire retardancy,[48] corrosion resistance,[49] etc.

In the previous sections, an industrially viable strategy to minimise the thickness and maximise the lateral dimensions of FLG/GNP particle has been presented. **Figure 5.a** compares the morphology (thickness and aspect ratio) of the best *in-situ* exfoliated FLG/GNP particles of this work (Protocol III-3) with the most representative results reported in the literature [17, 21, 23, 29, 34, 50-57] and commercially[58,59]. It can be seen that our *in-situ* exfoliated FLG/GNP have comparable thicknesses than average reported values (5 nm compared to minimum values of 1-3 nm), and generally higher aspect ratios (up to 1000 compared to ~200). It should be noted that our results are averages obtained without any process (centrifugation,[17] sedimentation,[29] etc.) of particle selection on the basis of their size, as often used and reported in literature. In other words we attain full conversion of the initial natural graphite (100 % yield, **Figure 5.a**) without any losses. To the best of our knowledge no other methodology achieves a comparable combination of production yield and size (aspect ratio and thickness).

The question remains how these interesting topological features and 'quality' of our *in-situ* exfoliated FLG/GNP particles translate into macroscopic properties of epoxy based nanocomposites.

Figure 5.c compares the bending elastic moduli of epoxy based nanocomposites filled with FLG/GNP particles obtained with Protocol III-3, as a function of filler content.[33, 60-75] To put these results into context, the mechanical reinforcement achieved (defined as $(E_C-E_M)/E_M$, where E_C and E_M are the flexural moduli of the composites and neat matrix, respectively) is compared with the best results found in the scientific literature for epoxy/graphitic particles nanocomposites. Interestingly, our FLG/GNP particles achieve the highest mechanical reinforcement ever reported, demonstrating the potential of our *in-situ* exfoliation process in

future applications. This is also the consequence of a very homogenous dispersion of the nanoparticles in epoxy, as shown in **Figure 5.b**.

Figure 5.d shows the electrical conductivity values of epoxy based nanocomposites filled with FLG/GNP particles obtained with Protocol III-3, compared with literature.[33, 67, 76-83] With a max electrical conductivity (relative to 5 wt.% of FLG/GNP) exceeding 10^{-2} S/m and a percolation threshold of ~ 1 wt.% our epoxy nanocomposites closely approach the best results ever reported in the literature (~ 10^{-1} S/m and ~ 0.5 wt.%, respectively).

It is noted that for sake of brevity only a limited number of results from the scientific and commercial literature could be used for comparison. A more complete collection of experimental data is included in our Supporting Information (**Table S1-2**).

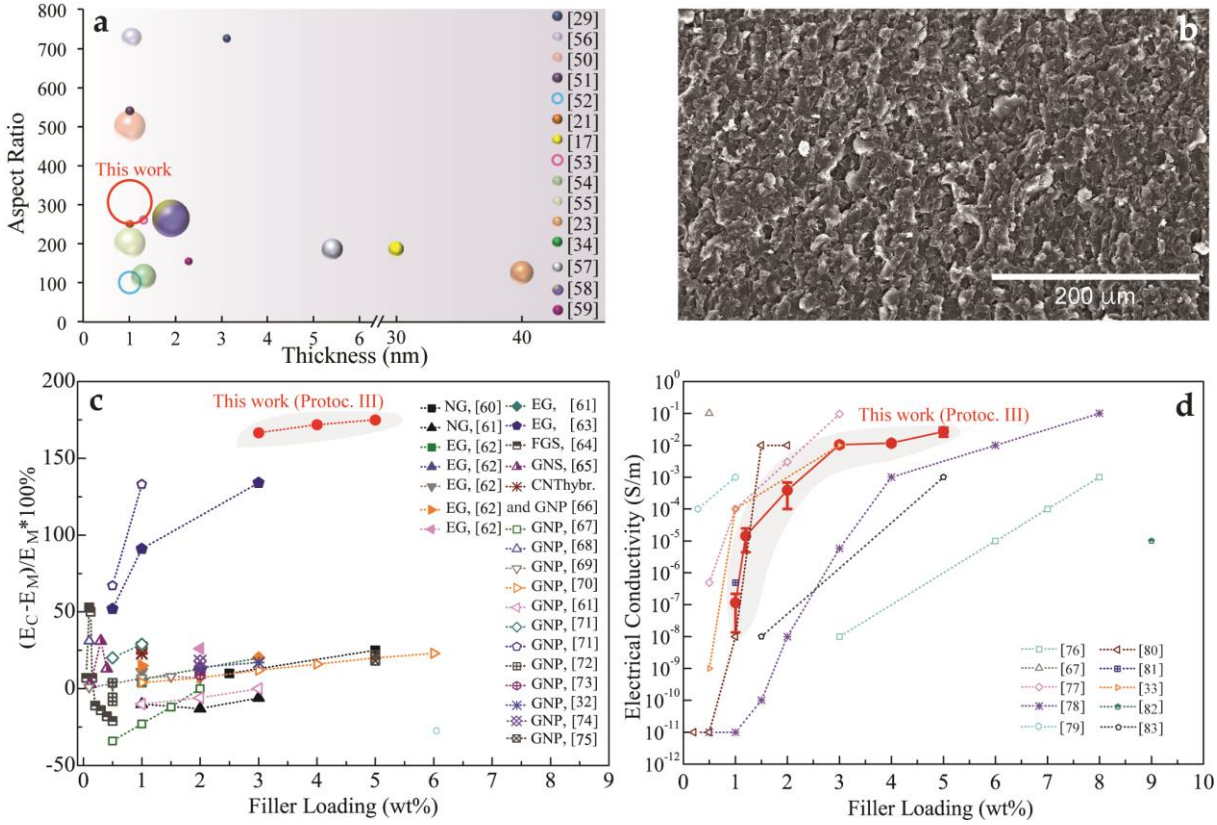

Figure 5. a) Comparison of morphological features (thickness, aspect ratio) and yield of *in-situ* exfoliated FLG/GNP produced by Protocol III-3 with graphitic nanoparticles from literature, b) SEM micrograph of the cross-sectional area of an epoxy nanocomposite containing with 5 wt.% FLG/GNP, produced by Protocol III-3, c) relative percentage increase in bending elastic moduli

of epoxy nanocomposite, produced by Protocol III-3, compared with literature, d) Electrical percolation curve of epoxy nanocomposite, produced by Protocol III-3, compared with literature.

CONCLUSIONS

For the first time the direct *in-situ* exfoliation and dispersion of FLG/GNP into epoxy resins was demonstrated, without the need of any additives, solvents, compatibilisers or chemical treatments. This single step, top-down, scalable and high yield (100% conversion of natural graphite) process promises to alleviate the cost barrier which is currently preventing the industrial uptake of graphene in bulk applications like composites and adhesives. Good quality (low defects; I_D/I_G ~0.07) FLG/GNP particles with an average aspect ratio greater than 300 and an average thickness of 5 nm were produced by fine tuning two important parameters: shear loading and temperature. Control over the first parameter resulted in an improved particle aspect ratio achieved by balancing the desirable reduction of particle thickness (delamination or exfoliation) with the inevitable particle break-down and reduction of lateral size (fracture). The second parameter was shown to improve the dispersion of the graphene nanoparticles while they are produced by mechanically exfoliation, due to a better matching of the surface energies of the graphite and liquid epoxy.

The above conclusions are interpreted in terms of simple energy balances and geometrical arguments, an analytical model of the TRM process and the Hansen solubility parameters.

The optimisation of the *in-situ* FLG/GNP particles morphology and 'quality' had a clear impact on macroscopic physical properties of the epoxy nanocomposites. An electrical percolation threshold of about 1 wt.% and an electrical conductivity exceeding 10^{-2} S/m were measured for particles obtained with the best processing conditions found. Aspect ratio had also a significant effect on mechanical properties, with the bending elastic modulus increasing by ~160 % for 4 wt.% of optimised FLG flakes, corresponding to the highest mechanical reinforcement ever reported for epoxy/graphene nanocomposites.

ASSOCIATED CONTENT

Supporting Information

This material is available free of charge *via* the Internet at http://pubs.acs.org.

Supporting Information content: Modelling of the TRL calendaring process; Rheology of epoxy resin; Surface tension measurements; Morphology of particles; Review of graphitic nanoparticles and their composites properties; Summary of processing parameters.

AUTHOR INFORMATION

Corresponding Authors

* Email (Emiliano Bilotti): e.bilotti@qmul.ac.uk
* Email (Ton Peijs): t.peijs@qmul.ac.uk

Notes

The authors declare no competing financial interest.

ACKNOWLEDGEMENTS

This research has received funding from Nanosynth Project which is funded by Innovate UK through the Technology Inspired Innovation – NANO Competition; project number: 101257. Yan Li would like to acknowledge financial support through the China Scholarship Council (CSC). NMP is supported by the European Research Council (ERC StG Ideas 2011 BIHSNAM no. 279985, ERC PoC 2015 SILKENE No. 693670) and by the European Commission under the Graphene Flagship (WP14 'Polymer Composites', No. 696656).

REFERENCES

1. Huang, X.; Qi, X.; Boey, F.; Zhang, H., Graphene-Based Composites. *Chem. Soc. Rev.* **2012,** *41* (2), 666-686.

2. Nika, D.; Ghosh, S.; Pokatilov, E.; Balandin, A., Lattice Thermal Conductivity of Graphene Flakes: Comparison with Bulk Graphite. *Appl. Phys. Lett.* **2009,** *94* (20), 1-3.

3. Morozov, S.; Novoselov, K.; Katsnelson, M.; Schedin, F.; Elias, D.; Jaszczak, J.; Geim, A., Giant Intrinsic Carrier Mobilities in Graphene and Its Bilayer. *Phys. Rev. Lett.* **2008,** *100* (1), 1-5.

4. Lee, C.; Wei, X.; Kysar, J. W.; Hone, J., Measurement of the Elastic Properties and Intrinsic Strength of Monolayer Graphene. *Science* **2008,** *321* (5887), 385-388.

5. Berry, V., Impermeability of Graphene and Its Applications. *Carbon* **2013,** *62*, 1-10.

6. Villar-Rodil, S.; Paredes, J. I.; Martínez-Alonso, A.; Tascón, J. M., Preparation of Graphene Dispersions and Graphene-polymer Composites in Organic Media. *J. Mater. Chem.* **2009,** *19* (22), 3591-3593.

7. Stankovich, S.; Dikin, D. A.; Dommett, G. H.; Kohlhaas, K. M.; Zimney, E. J.; Stach, E. A.; Piner, R. D.; Nguyen, S. T.; Ruoff, R. S., Graphene-based Composite Materials. *Nature* **2006,** *442* (7100), 282-286.

8. Hill, E. W.; Vijayaragahvan, A.; Novoselov, K., Graphene Sensors. *IEEE Sens. J.* **2011,** *11* (12), 3161-3170.

9. Gu, T.; Petrone, N.; Mcmillan, J. F.; Van Der Zande, A.; Yu, M.; Lo, G.-Q.; Kwong, D.-L.; Hone, J.; Wong, C. W., Regenerative Oscillation and Four-Wave Mixing in Graphene Optoelectronics. *Nat. Photonics* **2012,** *6* (8), 554-559.

10. Yoo, J. J.; Balakrishnan, K.; Huang, J.; Meunier, V.; Sumpter, B. G.; Srivastava, A.; Conway, M.; Mohana Reddy, A. L.; Yu, J.; Vajtai, R., Ultrathin Planar Graphene Supercapacitors. *Nano Lett.* **2011,** *11* (4), 1423-1427.

11. Wei, Z.; Wang, D.; Kim, S.; Kim, S.-Y.; Hu, Y.; Yakes, M. K.; Laracuente, A. R.; Dai, Z.; Marder, S. R.; Berger, C., Nanoscale Tunable Reduction of Graphene Oxide for Graphene Electronics. *Science* **2010,** *328* (5984), 1373-1376.

12. Xie, S.; Zhang, B.; Wang, C.; Wang, Z.; Li, L.; Li, J., Building Up Graphene-based Conductive Polymer Composite Thin Films Using Reduced Graphene Oxide Prepared by γ-Ray Irradiation. *Sci. World J.* **2013,** *2013*, 1-7.

13. Ataca, C.; Aktürk, E.; Ciraci, S.; Ustunel, H., High-capacity Hydrogen Storage by Metallized Graphene. *Appl. Phys. Lett.* **2008,** *93* (4), 043123.

14. Gong, L.; Young, R. J.; Kinloch, I. A.; Riaz, I.; Jalil, R.; Novoselov, K. S., Optimizing the Reinforcement of Polymer-based Nanocomposites by Graphene. *ACS Nano* **2012,** *6* (3), 2086-2095.

15. Young, R. J.; Kinloch, I. A.; Gong, L.; Novoselov, K. S., The Mechanics of Graphene Nanocomposites: A Review. *Compos. Sci. Technol.* **2012,** *72* (12), 1459-1476.

16. Chen, J.; Yao, B.; Li, C.; Shi, G., An Improved Hummers Method for Eco-Friendly Synthesis of Graphene Oxide. *Carbon* **2013,** *64*, 225-229.

17. Hernandez, Y.; Nicolosi, V.; Lotya, M.; Blighe, F. M.; Sun, Z.; De, S.; Mcgovern, I.; Holland, B.; Byrne, M.; Gun'Ko, Y. K., High-yield Production of Graphene by Liquid-phase Exfoliation of Graphite. *Nat. Nanotechnol.* **2008,** *3* (9), 563-568.

18. Lu, J.; Yang, J.-X.; Wang, J.; Lim, A.; Wang, S.; Loh, K. P., One-pot Synthesis of Fluorescent Carbon Nanoribbons, Nanoparticles, and Graphene by the Exfoliation of Graphite in Ionic Liquids. *ACS Nano* **2009,** *3* (8), 2367-2375.

19. Najafabadi, A. T.; Gyenge, E., High-yield Graphene Production by Electrochemical Exfoliation of Graphite: Novel Ionic Liquid (IL)–Acetonitrile Electrolyte with Low IL Content. *Carbon* **2014,** *71*, 58-69.

20. Yi, M.; Shen, Z.; Zhang, X.; Ma, S., Achieving Concentrated Graphene Dispersions in Water/Acetone Mixtures by the Strategy of Tailoring Hansen Solubility Parameters. *J. Phys. D: Appl. Phys.* **2012,** *46* (2), 1-9.

21. Lotya, M.; Hernandez, Y.; King, P. J.; Smith, R. J.; Nicolosi, V.; Karlsson, L. S.; Blighe, F. M.; De, S.; Wang, Z.; Mcgovern, I., Liquid Phase Production of Graphene by Exfoliation of Graphite in Surfactant/Water Solutions. *J. Am. Chem. Soc.* **2009,** *131* (10), 3611-3620.

22. Paton, K. R.; Varrla, E.; Backes, C.; Smith, R. J.; Khan, U.; O'Neill, A.; Boland, C.; Lotya, M.; Istrate, O. M.; King, P., Scalable Production of Large Quantities of Defect-free Few-layer Graphene by Shear Exfoliation in Liquids. *Nat. Mater.* **2014,** *13* (6), 624-630.

23. Chen, J.; Duan, M.; Chen, G., Continuous Mechanical Exfoliation of Graphene Sheets via Three-Roll Mill. *J. Mater. Chem.* **2012,** *22* (37), 19625-19628.

24. Ma, J.; Liu, R.; Wang, X.; Liu, Q.; Chen, Y.; Valle, R. P.; Zuo, Y. Y.; Xia, T.; Liu, S., Crucial Role of Lateral Size for Graphene Oxide in Activating Macrophages and Stimulating Pro-inflammatory Responses in Cells and Animals. *ACS Nano* **2015,** *9* (10), 10498-10515.

25. Liu, S.; Hu, M.; Zeng, T. H.; Wu, R.; Jiang, R.; Wei, J.; Wang, L.; Kong, J.; Chen, Y., Lateral Dimension-dependent Antibacterial Activity of Graphene Oxide Sheets. *Langmuir* **2012,** *28* (33), 12364-12372.

26. Gómez-Navarro, C.; Burghard, M.; Kern, K., Elastic Properties of Chemically Derived Single Graphene Sheets. *Nano Lett.* **2008,** *8* (7), 2045-2049.

27. Mahanta, N. K.; Abramson, A. R. In Thermal Conductivity of Graphene and Graphene Oxide Nanoplatelets, IEEE Intersoc. Conf. Therm. Thermomech. Phenom. Electron. Syst. **2012**; *2012*, 1-6.

28. Gómez-Navarro, C.; Weitz, R. T.; Bittner, A. M.; Scolari, M.; Mews, A.; Burghard, M.; Kern, K., Electronic Transport Properties of Individual Chemically Reduced Graphene Oxide Sheets. *Nano Lett.* **2007,** *7* (11), 3499-3503.

29. Khan, U.; O'Neill, A.; Porwal, H.; May, P.; Nawaz, K.; Coleman, J. N., Size Selection of Dispersed, Exfoliated Graphene Flakes by Controlled Centrifugation. *Carbon* **2012,** *50* (2), 470-475.

30. Rosca, I. D.; Hoa, S. V., Highly Conductive Multiwall Carbon Nanotube and Epoxy Composites Produced by Three-Roll Milling. *Carbon* **2009,** *47* (8), 1958-1968.

31. Kim, B. C.; Park, S. W.; Lee, D. G., Fracture Toughness of the Nano-particle Reinforced Epoxy Composite. *Compos. Struct.* **2008,** *86* (1), 69-77.

32. Moriche, R.; Prolongo, S.; Sánchez, M.; Jiménez-Suárez, A.; Sayagués, M.; Ureña, A., Morphological Changes on Graphene Nanoplatelets Induced During Dispersion into an Epoxy Resin by Different Methods. *Composites Part B* **2014**. *72*, 199-205.

33. Throckmorton, J.; Palmese, G., Direct Preparation of Few Layer Graphene Epoxy Nanocomposites from Untreated Flake Graphite. *ACS Appl. Mater. Interfaces* **2015,** *7* (27), 14870-14877.

34. Raza, M.; Westwood, A.; Brown, A.; Stirling, C., Texture, Transport and Mechanical Properties of Graphite Nanoplatelet/Silicone Composites Produced by Three Roll Mill. *Compos. Sci. Technol.* **2012,** *72* (3), 467-475.

35. Raza, M. A.; Westwood, A.; Brown, A.; Hondow, N.; Stirling, C., Characterisation of Graphite Nanoplatelets and the Physical Properties of Graphite Nanoplatelet/Silicone Composites for Thermal Interface Applications. *Carbon* **2011,** *49* (13), 4269-4279.

36. Magnier, R.; Agassant, J.-F.; Bastin, P., Experiments and Modelling of Calender Processing for Shear Thinning Thermoplastics between Counter Rotating Rolls with Differential Velocities. *Int. Polym. Process.* **2013,** *28* (4), 437-446.

37. Mackelvey, J. M., Polymer Processing. Wiley. **1962**.

38. Hildebrand, J. H.; Prausnitz, J. M.; Scott, R. L., Regular and Related Solutions. The Solubility Of Gases, Liquids, and Solids. Van Nostrand Reinhold New York. **1970**.

39. Hansen, C. M., Hansen Solubility Parameters: A User's Handbook. CRC Press. **2007**.

40. Abbott, S.; Hansen, C. M., Hansen Solubility Parameters in Practice. Hansen-Solubility. **2008**.

41. Hernandez, Y.; Lotya, M.; Rickard, D.; Bergin, S. D.; Coleman, J. N., Measurement of Multicomponent Solubility Parameters for Graphene Facilitates Solvent Discovery. *Langmuir* **2009,** *26* (5), 3208-3213.

42. Launay, H.; Hansen, C. M.; Almdal, K., Hansen Solubility Parameters for a Carbon Fiber/Epoxy Composite. *Carbon* **2007,** *45* (15), 2859-2865.

43. Sellam, C.; Zhai, Z.; Zahabi, H.; Picot, O. T.; Deng, H.; Fu, Q.; Bilotti, E.; Peijs, T., High Mechanical Reinforcing Efficiency of Layered Poly (Vinyl Alcohol)-Graphene Oxide Nanocomposites. *Nanocomposites* **2015,** *1* (2), 89-95.

44. Tandon, G.; Weng, G., The Effect of Aspect Ratio of Inclusions on the Elastic Properties of Unidirectionally Aligned Composites. *Compos. Polym.* **1984,** *5* (4), 327-333.

45. Yi, J. Y.; Choi, G. M., Percolation Behavior of Conductor-Insulator Composites with Varying Aspect Ratio of Conductive Fiber. *J. Electroceram.* **1999,** *3* (4), 361-369.

46. Wu, D.; Wu, L.; Zhou, W.; Sun, Y.; Zhang, M., Relations Between the Aspect Ratio of Carbon Nanotubes and the Formation of Percolation Networks in Biodegradable Polylactide/Carbon Nanotube Composites. *J. Polym. Sci., Part B: Polym. Phys.* **2010,** *48* (4), 479-489.

47. Lu, C.; Mai, Y.-W., Influence of Aspect Ratio on Barrier Properties of Polymer-Clay Nanocomposites. *Phys. Rev. Lett.* **2005,** *95* (8), 088303.

48. Cipiriano, B. H.; Kashiwagi, T.; Raghavan, S. R.; Yang, Y.; Grulke, E. A.; Yamamoto, K.; Shields, J. R.; Douglas, J. F., Effects of Aspect Ratio of MWNT on the Flammability Properties of Polymer Nanocomposites. *Polymer* **2007,** *48* (20), 6086-6096.

49. Zuo, Y.; Wang, H.; Xiong, J., The Aspect Ratio of Surface Grooves and Metastable Pitting of Stainless Steel. *Corros. Sci.* **2002,** *44* (1), 25-35.

50. Alanyalıoğlu, M.; Segura, J. J.; Oro-Sole, J.; Casan-Pastor, N., The Synthesis of Graphene Sheets with Controlled Thickness and Order Using Surfactant-Assisted Electrochemical Processes. *Carbon* **2012,** *50* (1), 142-152.

51. Khan, U.; O'Neill, A.; Lotya, M.; De, S.; Coleman, J. N., High-concentration Solvent Exfoliation of Graphene. *Small* **2010,** *6* (7), 864-871.

52. Green, A. A.; Hersam, M. C., Solution Phase Production of Graphene with Controlled Thickness via Density Differentiation. *Nano Lett.* **2009,** *9* (12), 4031-4036.

53. Yi, M.; Shen, Z.; Zhang, X.; Ma, S., Achieving Concentrated Graphene Dispersions in Water/Acetone Mixtures by the Strategy of Tailoring Hansen Solubility Parameters. *J. Phys. D: Appl. Phys.* **2013,** *46* (2), 025301.

54. Zhao, W.; Fang, M.; Wu, F.; Wu, H.; Wang, L.; Chen, G., Preparation of Graphene by Exfoliation of Graphite Using Wet Ball Milling. *J. Mater. Chem.* **2010,** *20* (28), 5817-5819.

55. Zhao, W.; Wu, F.; Wu, H.; Chen, G., Preparation of Colloidal Dispersions of Graphene Sheets in Organic Solvents by Using Ball Milling. *J. Nanomater.* **2010,** *2010*, 6.

56. Khan, U.; Porwal, H.; O'Neill, A.; Nawaz, K.; May, P.; Coleman, J. N., Solvent-exfoliated Graphene at Extremely High Concentration. *Langmuir* **2011,** *27* (15), 9077-9082.

57. Cho, D.; Lee, S.; Yang, G.; Fukushima, H.; Drzal, L. T., Dynamic Mechanical and Thermal Properties of Phenylethynyl ‐ Terminated Polyimide Composites Reinforced with Expanded Graphite Nanoplatelets. *Macromol. Mater. Eng.* **2005,** *290* (3), 179-187.

58. Http://Grapheneplatform.Com/

59. Http://Www.Thomas-Swan.Co.Uk/Advanced-Materials/Elicarb%C2%AE-Graphene-Products/Elicarb%C2%AE-Graphene

60. Yasmin, A.; Daniel, I. M., Mechanical and Thermal Properties of Graphite Platelet/Epoxy Composites. *Polymer* **2004,** *45* (24), 8211-8219.

61. Corcione, C. E.; Freuli, F.; Maffezzoli, A., The Aspect Ratio of Epoxy Matrix Nanocomposites Reinforced with Graphene Stacks. *Polym. Eng. Sci.* **2013,** *53* (3), 531-539.

62. Yasmin, A.; Luo, J.-J.; Daniel, I. M., Processing of Expanded Graphite Reinforced Polymer Nanocomposites. *Compos. Sci. Technol.* **2006,** *66* (9), 1182-1189.

63. Miller, S. G.; Bauer, J. L.; Maryanski, M. J.; Heimann, P. J.; Barlow, J. P.; Gosau, J.-M.; Allred, R. E., Characterization of Epoxy Functionalized Graphite Nanoparticles and the Physical Properties of Epoxy Matrix Nanocomposites. *Compos. Sci. Technol.* **2010,** *70* (7), 1120-1125.

64. Rafiee, M. A.; Rafiee, J.; Srivastava, I.; Wang, Z.; Song, H.; Yu, Z. Z.; Koratkar, N., Fracture and Fatigue in Graphene Nanocomposites. *Small* **2010,** *6* (2), 179-183.

65. Rafiee, M. A.; Lu, W.; Thomas, A. V.; Zandiatashbar, A.; Rafiee, J.; Tour, J. M.; Koratkar, N. A., Graphene Nanoribbon Composites. *ACS Nano* **2010,** *4* (12), 7415-7420.

66. Yang, S.-Y.; Lin, W.-N.; Huang, Y.-L.; Tien, H.-W.; Wang, J.-Y.; Ma, C.-C. M.; Li, S.-M.; Wang, Y.-S., Synergetic Effects of Graphene Platelets and Carbon Nanotubes on the Mechanical and Thermal Properties of Epoxy Composites. *Carbon* **2011,** *49* (3), 793-803.

67. Saw, W. S.; Mariatti, M., Properties of Synthetic Diamond and Graphene Nanoplatelet-filled Epoxy Thin Film Composites for Electronic Applications. *J. Mater. Sci.: Mater. Electron.* **2012,** *23* (4), 817-824.

68. Rafiee, M. A.; Rafiee, J.; Wang, Z.; Song, H.; Yu, Z.-Z.; Koratkar, N., Enhanced Mechanical Properties of Nanocomposites at Low Graphene Content. *ACS Nano* **2009,** *3* (12), 3884-3890.

69. Chatterjee, S.; Wang, J.; Kuo, W.; Tai, N.; Salzmann, C.; Li, W.; Hollertz, R.; Nüesch, F.; Chu, B., Mechanical Reinforcement and Thermal Conductivity in Expanded Graphene Nanoplatelets Reinforced Epoxy Composites. *Chem. Phys. Lett.* **2012,** *531*, 6-10.

70. King, J. A.; Klimek, D. R.; Miskioglu, I.; Odegard, G. M., Mechanical Properties of Graphene Nanoplatelet/Epoxy Composites. *J. Appl. Polym. Sci.* **2013,** *128* (6), 4217-4223.

71. Yang, Y.; Rigdon, W.; Huang, X.; Li, X., Enhancing Graphene Reinforcing Potential in Composites by Hydrogen Passivation Induced Dispersion. *Sci. Rep.* **2013,** *2086(3)*,1-7.

72. Prolongo, S.; Jimenez-Suarez, A.; Moriche, R.; Ureña, A., In Situ Processing of Epoxy Composites Reinforced with Graphene Nanoplatelets. *Compos. Sci. Technol.* **2013,** *86*, 185-191.

73. Ahmadi-Moghadam, B.; Taheri, F., Effect of Processing Parameters on the Structure and Multi-Functional Performance of Epoxy/GNP-Nanocomposites. *J. Mater. Sci.* **2014,** *49* (18), 6180-6190.

74. Wang, F.; Drzal, L. T.; Qin, Y.; Huang, Z., Effects of Functionalized Graphene Nanoplatelets on the Morphology and Properties of Epoxy Resins. *High Perform. Polym.* **2015**, *2015*,1-12.

75. Bose, S.; Drzal, L. T. Functionalization of Graphene Nanoplatelets Using Sugar Azide for Graphene/Epoxy Nanocomposites; DTIC Document: **2014**.1-22

76. Jović, N.; Dudić, D.; Montone, A.; Antisari, M. V.; Mitrić, M.; Djoković, V., Temperature Dependence of the Electrical Conductivity of Epoxy/Expanded Graphite Nanosheet Composites. *Scr. Mater.* **2008,** *58* (10), 846-849.

77. Monti, M.; Rallini, M.; Puglia, D.; Peponi, L.; Torre, L.; Kenny, J., Morphology and Electrical Properties of Graphene–Epoxy Nanocomposites Obtained by Different Solvent Assisted Processing Methods. *Composites Part A* **2013,** *46*, 166-172.

78. Wang, Y.; Yu, J.; Dai, W.; Song, Y.; Wang, D.; Zeng, L.; Jiang, N., Enhanced Thermal and Electrical Properties of Epoxy Composites Reinforced with Graphene Nanoplatelets. *Polym. Compos.* **2015,** *36* (3), 556-565.

79. Wajid, A. S.; Ahmed, H.; Das, S.; Irin, F.; Jankowski, A. F.; Green, M. J., High‐Performance Pristine Graphene/Epoxy Composites with Enhanced Mechanical and Electrical Properties. *Macromol. Mater. Eng.* **2013,** *298* (3), 339-347.

80. Li, J.; Vaisman, L.; Marom, G.; Kim, J.-K., Br Treated Graphite Nanoplatelets for Improved Electrical Conductivity of Polymer Composites. *Carbon* **2007,** *45* (4), 744-750.

81. Wei, T.; Song, L.; Zheng, C.; Wang, K.; Yan, J.; Shao, B.; Fan, Z.-J., The Synergy of a Three Filler Combination in the Conductivity of Epoxy Composites. *Mater. Lett.* **2010,** *64* (21), 2376-2379.

82. Gantayat, S.; Prusty, G.; Rout, D. R.; Swain, S. K., Expanded Graphite as a Filler for Epoxy Matrix Composites to Improve their Thermal, Mechanical and Electrical Properties. *New Carbon Mater.* **2015,** *30* (5), 432-437.

83. Lu, W.; Weng, J.; Wu, D.; Wu, C.; Chen, G., Epoxy Resin/Graphite Electrically Conductive Nanosheet Nanocomposite. *Mater. Manuf. Processes* **2006,** *21* (2), 167-171.